Supplementary Materials for "**Remineralization dominating the $\delta^{13}C$ decrease in the mid-depth Atlantic during the last deglaciation**"

Sifan Gu[1,2], Zhengyu Liu[3], Delia W. Oppo[4], Jean Lynch-Stieglitz[5], Alexandra Jahn[6], Jiaxu Zhang[7], Keith Lindsay[8], Lixin Wu[1,9]

[1] School of Oceanography, Shanghai Jiao Tong University, Shanghai, China

[2] Open Studio for Ocean-Climate-Isotope Modeling, Pilot National Laboratory for Marine Science and Technology (Qingdao), Qingdao, China

[3] Atmospheric Science Program, Department of Geography, The Ohio State University, Columbus, OH, USA

[4] Department of Geology and Geophysics, Woods Hole Oceanographic Institution, Woods Hole, MA, USA

[5] School of Earth and Atmospheric Sciences, Georgia Institute of Technology, Atlanta, Georgia, USA

[6] Department for Atmospheric and Oceanic Sciences and Institute of Arctic and Alpine Research, University of Colorado Boulder, Boulder, CO, USA

[7]

[8] National Center for Atmospheric Research, Climate and Global Dynamics Division, Boulder, CO, USA

[9] Pilot National Laboratory for Marine Science and Technology (Qingdao), Qingdao, China

Correspondence authors: Sifan Gu (gusifan@sjtu.edu.cn), Zhengyu Liu (liu.7022@osu.edu)

This file contains additional information about the methods and additional figures to the main manuscript.

Text 1. Remineralized $\delta^{13}C$ estimation from AOU

The remineralized $\delta^{13}C$ in POP2 can be estimated from AOU (Sarmiento and Gruber, 1996) as described below. Total DIC, which is mostly $DI^{12}C$, can be seperated into preformed DIC (DIC_{pre}) and remineralized DIC (DIC_{remin}):

$$DIC = DIC_{pre} + DIC_{rem} \quad \text{(eq. 1)}$$

The fractionation in POP2 involves organic fractionation and carbonate formation (eq.2), therefore, DIC_{rem} can be further decomposed into DIC related to the organic process (DIC_{org}) and DIC related to carbonate pricipitation (DIC_{CaCO3}):

$$DIC_{rem} = DIC_{org} + DIC_{CaCO3} \quad \text{(eq. 2)}$$

DIC_{org} can be estimated using AOU by:

$$DIC_{org} = r_{C:O}*AOU \quad \text{(eq. 3)}$$

where $r_{C:O}$ is the ratio of carbon to oxygen during the organic process and is set to 117/138 in the model. DIC_{CaCO3} can be estimated as:

$DIC_{CaCO3} = (ALK - ALK_{pre} + r_{N:O}*AOU)/2$ (eq. 4),

where ALK is alklinity, ALK_{pre} is preformed alklinity, and $r_{N:O}$ is the ratio of nitrate to oxygen during the organic process which is 16/170. The ALK_{pre} can be estimated by:

$ALK_{pre} = (367.5 + 54.9*S + 0.074*(O_2 + r_{O:P}*PO_4))$ (eq. 5),

where S is salinity, O_2 is oxygen concentration, PO_4 is phosphate concentraion, and $r_{O:P}$ is the ratio of oxygen and phosphahte during the organic process which is 170. Combinating equation 1-5, the DIC_{pre} can be calculated by: $DIC_{pre} = DIC - DIC_{org} – DIC_{CaCO3}$ (eq. 6).

The fractionation during the organic process ($\delta^{13}C_{org}$) is approximately -21‰ and the fractionation during the carbonate precipitation ($\delta^{13}C_{CaCO3}$) is 2‰. Therefore, the $\delta^{13}C_{pre}$ can be calculated by:

$$\delta^{13}C_{pre} = (\delta^{13}C* DIC - \delta^{13}C_{org}*DIC_{org} - \delta^{13}C_{CaCO3}* DIC_{CaCO3})/DIC_{pre} \quad \text{(eq.7)}$$

and the $\delta^{13}C_{remin}$ can be estimated by $\delta^{13}C - \delta^{13}C_{pre}$.

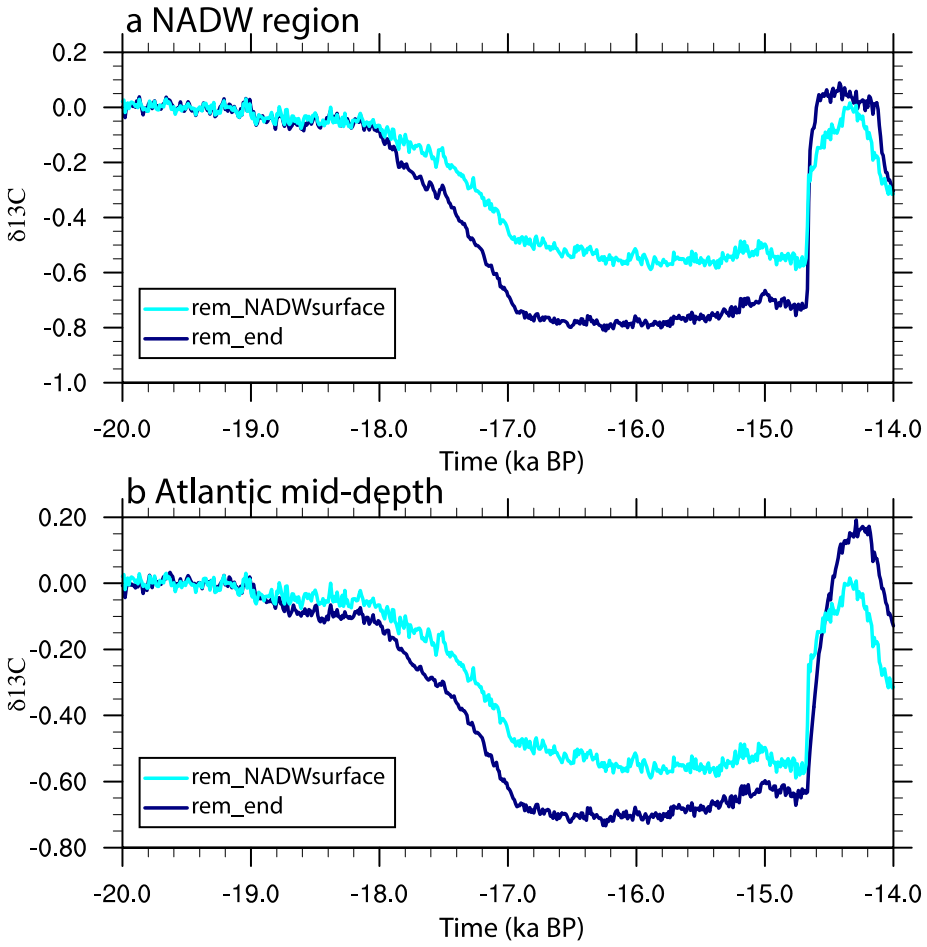

Figure S1. Validation of the $\delta^{13}C_{rem-end}$ estimation in NADW deep end-member region (a) and Atlantic mid-depth average (b): $\delta^{13}C_{rem-end}$ by the difference between $\delta^{13}C_{rem}$ and $\delta^{13}C_{rem-path}$ (navy); $\delta^{13}C_{rem}$ in the NADW surface end-member (light blue)

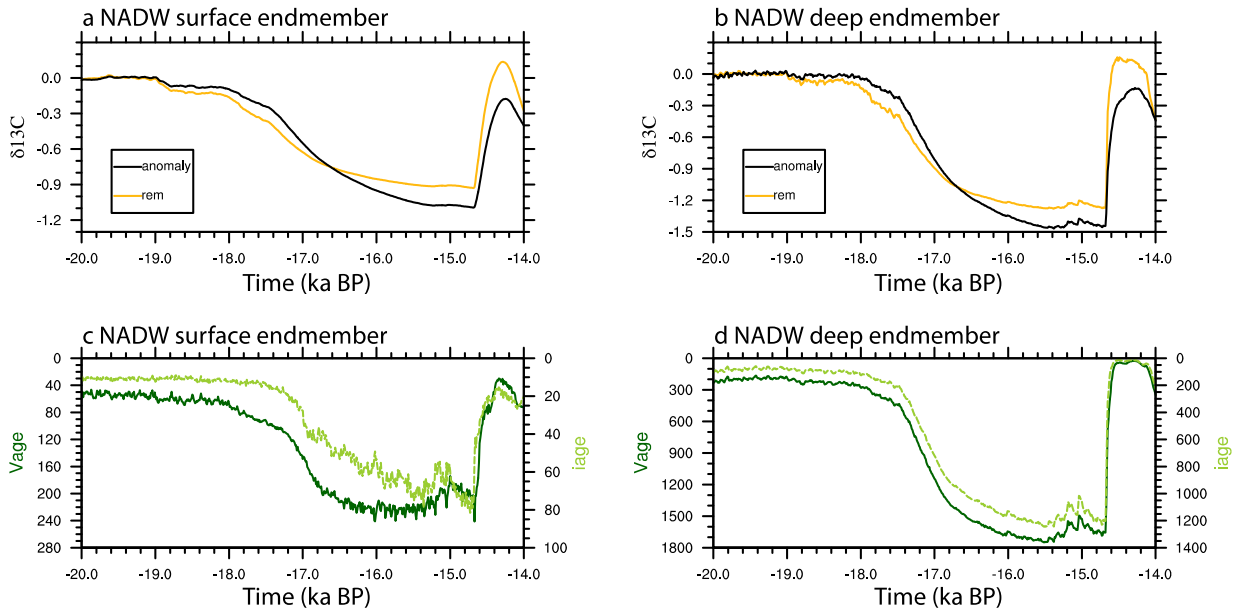

Figure S2. Evolutions in NADW surface and deep end-members. (a) $\delta^{13}C$ anomaly (black) and $\delta^{13}C_{rem}$ (yellow) of NADW surface end-member. (b) $\delta^{13}C$ anomaly (black) and $\delta^{13}C_{rem}$ (yellow) of NADW deep end-member. (c) Idealized ventilation age (dark solid green) and ideal age (light dashed green) in NADW surface endmember. (d) Idealized ventilation age (dark solid green) and ideal age (light dashed green) in NADW deep endmember.

Table S1. $\delta^{13}C$ observations used in model-data comparison.

site	Lat	lon	Depth (m)	$\delta^{13}C$ (HS1-LGM)	Reference
14GGC	-26.68	-46.5	441	0.0667	(Curry and Oppo, 2005)
90GGC	-27.35	-46.63	1105	0.332	(Curry and Oppo, 2005)
KNR159-5-36GGC	-27.27	-46.47	1268	0.14	(Curry and Oppo, 2005)
KNR159-5-17JPC	-27.7	-46.48	1627	-0.58	(Tessin and Lund, 2013)
KNR159-5-78GGC	-27.48	-46.33	1820	-0.48	(Tessin and Lund, 2013)
KNR159-5-33GGC	-27.57	-46.18	2082	-0.31	(Tessin and Lund, 2013)
KNR159-5-42JPC	-27.76	-46.63	2296	-0.32	(Curry and Oppo, 2005)
KNR159-5-73GGC	-27.89	-46.04	2397	-0.07	(Tessin and Lund, 2013)
KNR159-5-30GGC	-28.13	-46.04	2500	-0.19	(Tessin and Lund, 2013)

20JPC	-28.64	-45.54	2951	-0.2075	(Lund et al., 2015)
KNR159-5-125GGGC	-29.52	-45.75	3589	-0.2	(Hoffman and Lund, 2012)
KNR159-5-22GGGC	-29.79	-43.59	3924	0.15	(Hoffman and Lund, 2012)
GeoB3104-1	-3.66	-37.71	767	-0.008925	(Arz et al., 1999)
GS07-150-17	-4.21	-37.07	1000	-0.625	(Freeman et al., 2015)
GeoB16206-1	-1.58	-43.02	1367	-2.23	(Voigt et al., 2017)
GeoB1602-2	-1.91	-41.59	2247	-0.55769	(Mulitza et al., 2017)
GeoB3910-2	-4.25	-36.35	2362	-0.5842	(Burckel et al., 2015)
GeoB16224-1	6.65	-52.08	2510	-0.335833	(Voigt et al., 2017)
Rapid-10-1P	62.98	-17.59	1237	-0.86	(Thornalley et al., 2010)
EW9302-26GGC	62.32	-21.46	1450	-1.08	(Oppo et al., 2015)
EW9302-25GGC	62.06	-21.47	1523	-1.08	(Oppo et al., 2015)
NEAP4k	61.29	-24.17	1627	-0.88	(Rickaby and Elderfield, 2005)
EW9302-24GGC	62	-21.67	1629	-0.92	(Oppo et al., 2015)
ODP 984	61	-24	1648	-0.83	(Praetorius et al., 2008)
Rapid-15-4P	63.29	-17.13	2133	-0.27	(Thornalley et al., 2010)
RAPiD-17-5P	61.48	-19.54	2303	-0.38	(Thornalley et al., 2010)
KN166-14-JPC-13	53.06	-33.53	3082	-0.3	(Hodell et al., 2010)
IODP U1308	49.88	-24.24	3883	-0.25	(Hodell et al., 2008)

Reference:

Arz, H.W., Pätzold, J., Wefer, G., 1999. The deglacial history of the western tropical Atlantic as inferred from high resolution stable isotope records off northeastern Brazil. Earth Planet. Sci. Lett. 167, 105–117. https://doi.org/10.1016/S0012-821X(99)00025-4

Burckel, P., Waelbroeck, C., Gherardi, J.M., Pichat, S., Arz, H.W., Lippold, J., Dokken, T., Thil, F., 2015. Atlantic Ocean circulation changes preceded millennial tropical South America rainfall events during the last glacial. Geophys. Res. Lett. 42, 411–418. https://doi.org/10.1002/2014GL062512.Received

Curry, W.B., Oppo, D.W., 2005. Glacial water mass geometry and the distribution of δ13 C of ΣCO2 in the western Atlantic Ocean. Paleoceanography 20. https://doi.org/10.1029/2004PA001021

Freeman, E., Skinner, L.C., Tisserand, A., Dokken, T., Timmermann, A., Menviel, L., Friedrich,

T., 2015. An Atlantic-Pacific ventilation seesaw across the last deglaciation. Earth Planet. Sci. Lett. 424, 237–244. https://doi.org/10.1016/j.epsl.2015.05.032
Hodell, D.A., Channeil, J.E.T., Curtis, J.H., Romero, O.E., Röhl, U., 2008. Onset of "Hudson Strait" Heinrich events in the eastern North Atlantic at the end of the middle Pleistocene transition (~640 ka)? Paleoceanography 23, 1–16. https://doi.org/10.1029/2008PA001591
Hodell, D.A., Evans, H.F., Channell, J.E.T., Curtis, J.H., 2010. Phase relationships of North Atlantic ice-rafted debris and surface-deep climate proxies during the last glacial period. Quat. Sci. Rev. 29, 3875–3886. https://doi.org/10.1016/j.quascirev.2010.09.006
Hoffman, J.L., Lund, D.C., 2012. Refining the stable isotope budget for Antarctic Bottom Water: New foraminiferal data from the abyssal southwest Atlantic. Paleoceanography 27, 1–12. https://doi.org/10.1029/2011PA002216
Lund, D.C., Tessin, A.C., Hoffman, J.L., Schmittner, A., 2015. Southwest Atlantic water mass evolution during the last deglaciation. Paleoceanogr. Paleoclimatology 477–494. https://doi.org/10.1002/2014PA002657.Received
Mulitza, S., Chiessi, C.M., Schefuß, E., Lippold, J., Wichmann, D., Antz, B., Mackensen, A., Paul, A., Prange, M., Rehfeld, K., Werner, M., Bickert, T., Frank, N., Kuhnert, H., Lynch-Stieglitz, J., Portilho-Ramos, R.C., Sawakuchi, A.O., Schulz, M., Schwenk, T., Tiedemann, R., Vahlenkamp, M., Zhang, Y., 2017. Synchronous and proportional deglacial changes in Atlantic meridional overturning and northeast Brazilian precipitation. Paleoceanography 32, 622–633. https://doi.org/10.1002/2017PA003084
Oppo, D.W., Curry, W.B., McManus, J.F., 2015. What do benthic δ13C and δ18O data tell us about Atlantic circulation during Heinrich Stadial 1? Paleoceanography 30, 353–368. https://doi.org/10.1002/2014PA002667
Praetorius, S.K., McManus, J.F., Oppo, D.W., Curry, W.B., 2008. Episodic reductions in bottom-water currents since the last ice age. Nat. Geosci. 1, 449–452. https://doi.org/10.1038/ngeo227
Rickaby, R.E.M., Elderfield, H., 2005. Evidence from the high-latitude North Atlantic for variations in Antarctic Intermediate water flow during the last deglaciation. Geochemistry, Geophys. Geosystems 6. https://doi.org/10.1029/2004GC000858
Sarmiento, J.L., Gruber, N., 1996. Ocean Biogeochemical Dynamics.
Tessin, A.C., Lund, D.C., 2013. Isotopically depleted carbon in the mid-depth South Atlantic during the last deglaciation. Paleoceanography 28, 296–306. https://doi.org/10.1002/palo.20026
Thornalley, D.J.R., Elderfield, H., McCave, I.N., 2010. Intermediate and deep water paleoceanography of the northern North Atlantic over the past 21,000 years. Paleoceanography 25, PA1211. https://doi.org/10.1029/2009PA001833
Voigt, I., Cruz, A.P.S., Mulitza, S., Chiessi, C.M., Mackensen, A., Lippold, J., 2017. Variability in mid-depth ventilation of the western Atlantic Ocean during the last deglaciation. Palaeogeography 32, 1–27. https://doi.org/10.1002/2017PA003095